Basic Experiments for High-Torque, Low-Speed Permanent Magnet Synchronous Motor and a Technique for Reducing Cogging Torque

Kouichi Sato, Jung-Seob Shin, Takafumi Koseki and Yasuaki Aoyama

***Abstract* -- Fully integrated electric propulsion systems are gaining popularity in both commercial and military sectors. Propulsion motor manufacturers are investigating new direct drive solutions for use in electric ships. These applications require motors with high torque output at low speeds. Such requirements were the motivation for the design of a new PMSM with a novel topology. Firstly, this paper describes an efficient model of a motor used for high thrust at low speed. Secondly, the authors analyze the theory for motor's behavior. To compare the theoretical result, characteristics of the proposed motor have been tested. The cogging torque has been a serious problem. Therefore, an analytical model of the cogging torque has been derived for calculating and reducing it. An appropriate skew angle can be designed based on the model.**

***Index Terms*--permanent magnet synchronous motor (PMSM), transverse flux machine (TFM), tunnel actuator (TA), cogging torque, skew**

I. Introduction

As commercial automotive, aerospace, and railway industries were affected by rising fuel costs a couple of years ago, the marine industry has recently endeavored to create more fuel-efficient, cost-effective drive systems. During the last 15-20 years, fully electrified propulsion (EP) systems have been gaining popularity and capturing most of the market growth in sectors such as cruise ships, passenger ferries, oil and gas transport vessels, and merchant and special order ships [1]-[2]. Several different types of motors are currently in use or have been proposed for application in ship propulsion. The authors took particular interest in a Permanent Magnet Synchronous Motor (PMSM) solution because of the possibility of higher thrust, less complicated design, and lower maintenance.

Due to the short pole pitch characteristic of certain types of PMSM designs, these machines can have high torque at low speeds, which is particularly beneficial in a marine application. Transverse Flux Motor (TFM) designs have short pole pitch and high torque characteristics, but TFM are plagued by low power factor [3]-[4]. In order to improve on previous designs, the authors developed a theoretical model of a transverse flux PMSM and subsequently built and tested the prototype of a new design. The authors also adapted the basic flux path idea present in the Tunnel Actuator (TA), a linear PMSM produced by Hitachi, to perform in a rotary application. Also, in order to decrease the cogging torque that has a negative effect on behavior of a PMSM, the authors suggested the techniques with skew to reduce the cogging torque. Finally, to compare the theoretical result, the authors had an experiment on the characteristic of suggested motor.

II. Fundamentals of New Motor Design

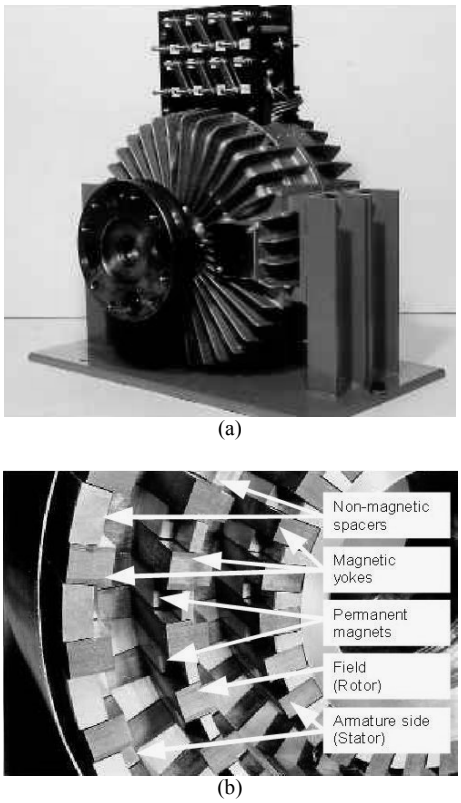

(a)

(b)

Fig. 1: Transverse Flux Machine

The transverse flux machine takes advantage of a 3-D flux path to increase torque production without having to trade off between electrical or magnetic loading as with radial and axial flux machines. But, the TFM described by Weh, et. al. and later improvements on that design have such complex manufacturing requirements that they are impractical for industrial production. This complex design can be seen in Fig. 1(a)-(b). Ultimately, the low power factor characteristic of transverse flux machines becomes an obstacle against this type of machine attaining a high real power to volume ratio. For example, Rolls-Royce Ltd. manufactured a TFM for marine propulsion that was capable of large thrust but had power factor ratings of less than 0.7 [6].

When examining the field of direct drives for another motor with a similar flux path configuration but a high power factor, the authors found Hitachi's Tunnel Actuator for linear drive applications [5]. This drive has the advantages of easy assembly, thin permanent magnet and high resultant permeability and a magnetic flux path that is transverse. The TA suffered from large flux leakage due to the close position of the armature poles and the

This work was supported by MT-Drive and Japan Society for the Promotion of Science.

Kouichi Sato, Jung-Seob Shin and Takafumi Koseki are with Department of Electrical Engineering and information systems, School of Engineering, The University of Tokyo, 7-3-1, Hongo, Bunkyo-ku, Tokyo 113-8656, Japan (e-mail: kouichi@koseki.t.u-tokyo.ac.jp).

Yasuaki Aoyama is with Hitachi Reseach Laboratory, Hitachi, Ltd., Ibaraki-ken, Japan.

configuration of the flux path in alternating poles. The authors thought that by placing only poles with flux in the same direction next to each other and spacing them further apart to increase magnetic isolation. The following sections will show the details of new direct drive design.

A. The Model

The basic unit of our model was one pole of the machine. One pole consists of a stator C-core. The winding is wrapped around the back of the C, and the permanent magnets on the rotor are accelerated through the air gap to generate thrust. An illustration of the one-pole model is in Fig. 2. The input to the model is the armature current I_a. B_a is the armature flux density and B_f is the flux density contributed by the field magnets. As I_a changes, the polarity of B_a also fluctuates, which pulls the alternating polarity magnets through the air gap, creating thrust. The movement of the magnets through the armature flux field also induces an internal EMF.

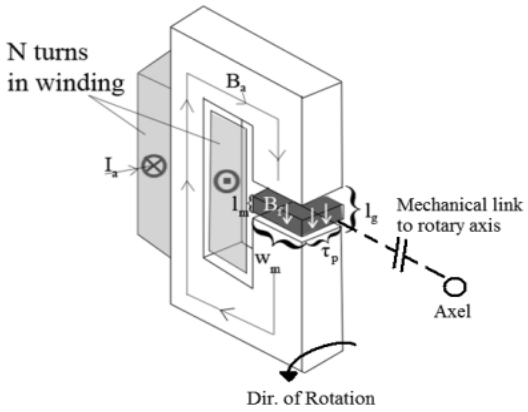

Fig. 2: One-Pole Model Diagram[7]

Fig. 3 shows how the rotor would be propelled through the consecutive air gaps of several poles connected in phase by their armature winding. The self-induced voltage and thrust contributed by each pole would be superimposed to create the total contribution of one phase. The phases of the machine could then be connected to the operator's convenience. The C-cores of each phase would be placed at balanced angular separation around the axel to create the outer radius of the machine.

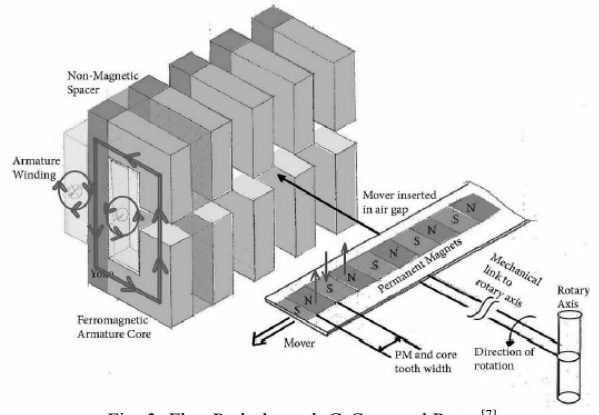

Fig. 3: Flux Path through C-Core and Rotor[7]

B. Creation of the Prototype and Test Bench

The prototype design was created by taking a number of unit model C-cores and arranging them radially to create a full stator. In Fig. 4(a)-(b), this idea is drawn up with 3-phases and 4 stator cores per phase. In the actual prototype, only 2 cores were used per phase. The rotor was constructed in a similar fashion by placing alternating polarity magnets on a rotor backing at a set angular separation. In the prototype, there were 36 permanent magnets, thus 18 pole pairs.

It is important to note that because the flux lines in adjacent stator cores of the same phase point in the same direction and there is a large physical separation between phases, the authors expected negligible flux leakage.

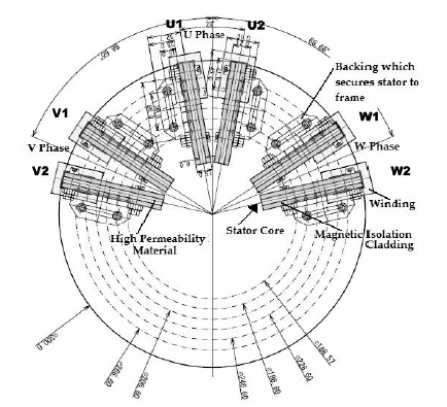

(a) Stator Cores

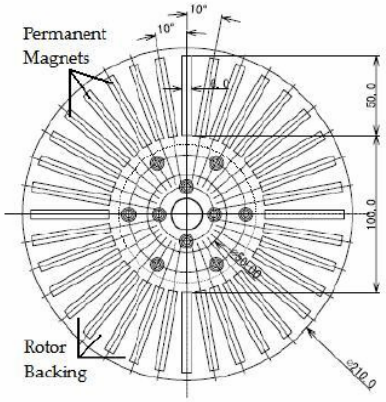

(b) Rotor

Fig. 4: Layout of the Prototype Motor Model[7]

Fig. 5-6 is detailed parts of the prototype motor and the full test bench involved directly connecting a PMSM load motor to the prototype. The prototype was driven directly in generator mode. The prototype was connected to an inverter to be controlled for dynamic testing. This test bench accurately represents the typical case of an industrial client, where the motor supplier will have only general knowledge about the loading conditions applied to their product [7].

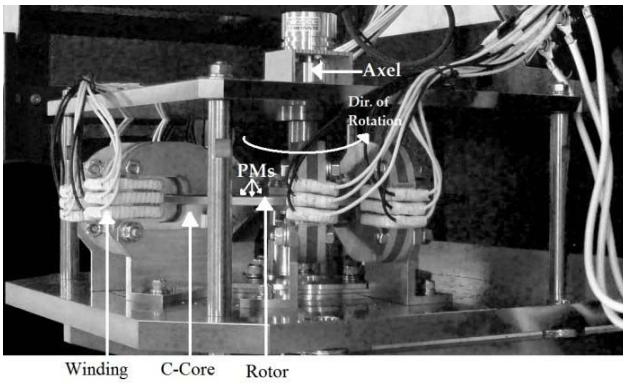

Fig. 5: Detailed Parts of the Prototype Motor[7]

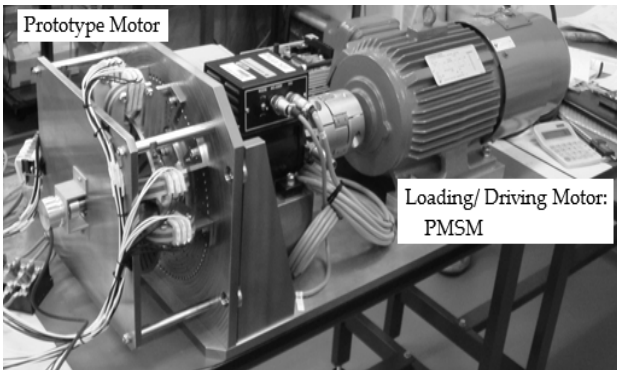

Fig. 6: A Full Version of the Prototype Motor Model[7]

III. FUNDAMENTAL EXPERIMENT

In order to verify how our design motor would behave, experiments measuring the fundamental characteristics of the prototype motor were preformed. To measure easily, the authors considered 1 core per one phase in the experiment.

A. Armature Resistance Measurement

By using DC-voltage drop test, armature resistance was measured. Fig. 7 shows the test circuit. Armature winding resistance is calculated from applied DC voltage V_{DC} and the current I. Three values of armature resistance (U, V, W phase) were measured. The experimental result is shown in Fig. 8.

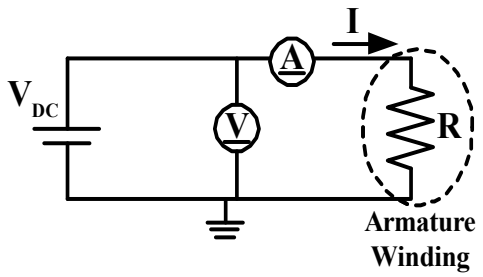

Fig. 7: DC-Voltage Drop Test Circuit

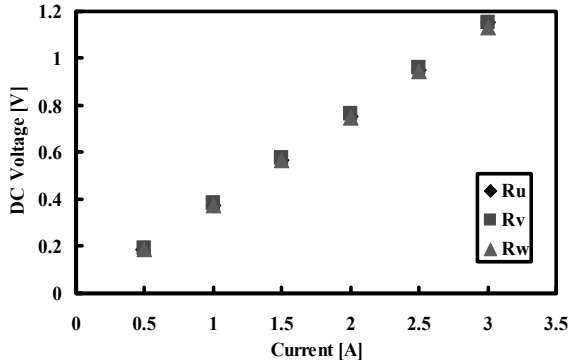

Fig. 8: Armature Resistance Measurement

As the experimental result shows, voltage was almost proportional to current and three armature resistances were corresponded. Average of three resistances is expressed as (1).

$$\overline{R} = \frac{R_u + R_v + R_w}{3} = 0.379 \quad [\Omega] \tag{1}$$

B. Self-Inductance Measurement

By using AC source V_{AC} and test resistance R_{test}, self-inductance was measured Fig. 9 shows the test circuit.

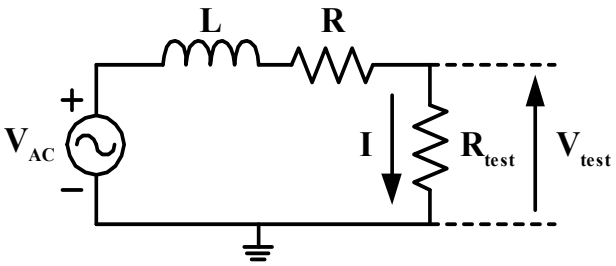

Fig. 9: The Test Circuit for Measuring Self-Inductance

As shown in Fig. 9, the test resistance was connected with the armature winding in the series, and the effective voltages, the phase differences of the test resistance and AC source were observed by oscilloscope. By using two effective voltages and the phase deference, AC resistance R and self-inductance L can be obtained. R was obtained in DC measurement. However, R was considered as a variable to obtain AC resistance accurately. Equations to obtain R and L are (2)-(3).

$$L = \frac{|V_{AC}|R_{test}\sin\theta}{2\pi f|V_{test}|} \tag{2}$$

$$R = R_{test}\left(\frac{|V_{AC}|}{|V_{test}|}\cos\theta - 1\right) \tag{3}$$

f is frequency (10~50 [Hz]) of AC source, and θ is a value converted from the phase deference. Based on these equations and the experimental result, R and L were calculated. The result is shown in Fig. 10-11.

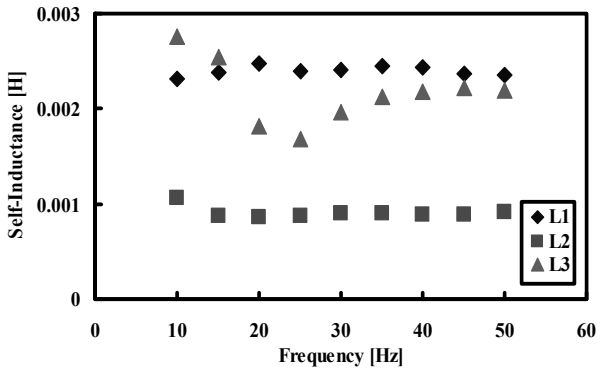

Fig. 10: Self-Inductance Measurement

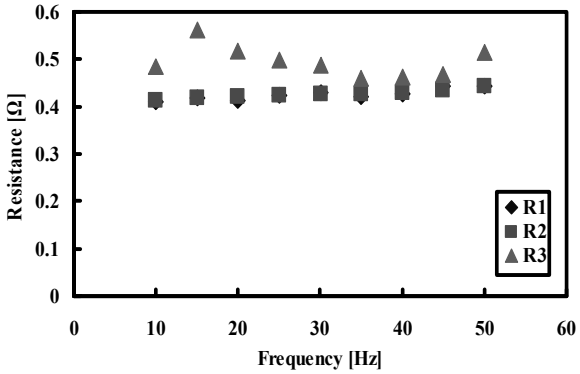

Fig. 11: AC Resistance Measurement

R_1 and L_1 are the value when there is nothing in gap. R_2 and L_2 are the value when permanent magnet is under the C-core in the air gap. Also, R_3 and L_3 are the value when stainless (metal between permanent magnets) is under the C-core in the air gap. Although R_1 and R_2 were almost corresponded, L_1 and L_2 depended on each pattern. R_3 and L_3

are unstable values especially in low frequency. In this pattern, the prototype motor was not stable and the experiment was performed holding the rotor by hand. AC resistance was larger than DC resistance. The authors guessed that the reason was due to the skin effect caused by AC component. However, since R and L don't almost depend on frequency except for R_3 and L_3, it can be considered that the experiment was good result. Theoretically, since the authors assumed that there was nothing in the air gap when calculating L, L_1 was used. Average of L_1 is expressed as (4).

$$L = \overline{L_1} = 2.40 \quad [\text{mH}] \tag{4}$$

C. Open Circuit Test

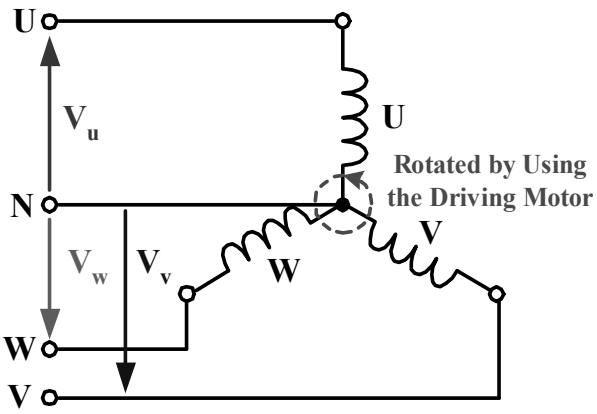

Fig. 12: The Test Circuit for Measuring Self-Induced Voltage

Self-induced voltage was measured by open circuit test. In this test, rotating speed could be controlled by connecting the prototype motor to the driving motor. And, self-induced voltage is measured by rotating the driving motor changing speed. Fig. 12 shows the test circuit. As shown in Fig. 12, the armature side was opened and the neutral point N was connected by distributed cable. In the experiment, rotating the prototype motor by driving motor, the effective voltages and the phase differences of each phase voltage were measured by oscilloscope. The test result is given in Fig. 13-14.

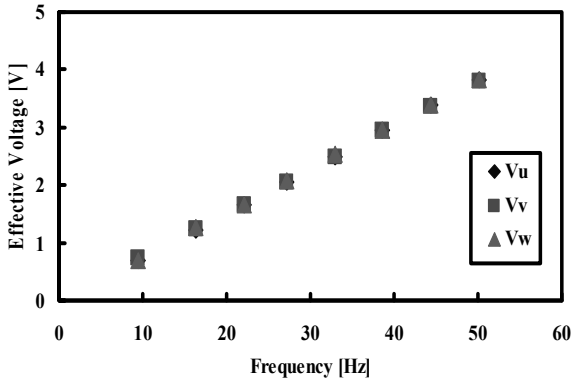

Fig. 13: Effective Voltage in the Open Circuit Test

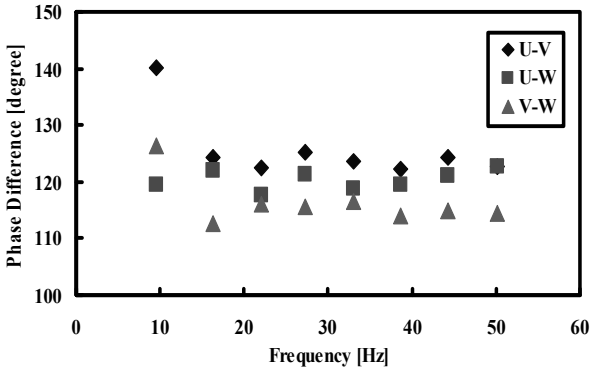

Fig. 14: Phase Difference in the Open Circuit Test

Theoretically, the effective voltage is proportional to frequency, and the phase differences of each phase is 120 [degree]. As shown in Fig. 13, three effective voltages were proportional to frequency and the values were almost corresponding with each frequency. When Frequency is 50 [Hz], averaged effective voltage is expressed as (5).

$$\overline{V_{rms}} = \frac{V_u + V_v + V_w}{3} = 3.81 \quad [\text{V}] \tag{5}$$

As shown in Fig. 14, the phase differences of each phase were fallen in error within about 5% of 120 [degree].

IV. Comparison of Theoretical and Empirical Data

By measuring fundamental characteristics, the armature winding resistance R, self-inductance L and self-induced voltage V_{rms} were gained. By using these values, the authors estimated specifications that indicate performance of the motor at nominal operating point. Assuming the condition when d-axis current is controlled to zero, they are expressed one phase equivalent circuit in Fig. 15 and phasor diagram of voltages and currents in Fig. 16. Based on these figures, the authors calculated specifications : output P, torque T, power factor $\cos\theta$, efficiency η, and force density D.

$$P = 3V_{rms}I_{rms} \tag{6}$$

$$T = \frac{P}{\omega_m} = \frac{P}{2\pi f} \cdot p \tag{7}$$

$$\cos\theta = \frac{V_{rms} + RI_{rms}}{\sqrt{(V_{rms} + RI_{rms})^2 + (XI_{rms})}} \tag{8}$$

$$\eta = \frac{V_{rms}}{V_{rms} + RI_{rms}} \tag{9}$$

$$D = \frac{T}{3rS} \tag{10}$$

In (6)-(10), I_{rms} is the current to be applied to the armature winding and p is pole pairs of permanent magnet. X is inductive reactance and r is average rotation radius, and S is cross-sectional area of pole. Table I shows the theoretical and empirical values for each parameter of the prototype motor.

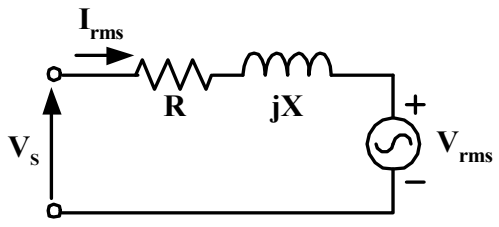

Fig. 15: One Phase Equivalent Circuit

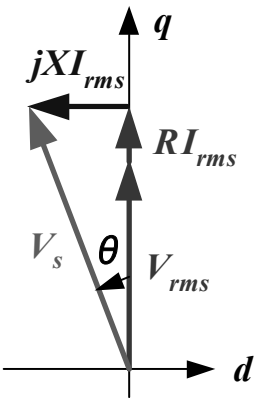

Fig. 16: Phasor Diagram of Voltages and Currents ($I_d = 0$)

TABLE I
COMPARISON OF THEORETICAL AND EMPIRICAL

Specification	Theoretical Value	Empirical Value
Winding Resistance : R	0.319 [Ω]	0.379 [Ω]
Self-Inductance : L	0.444 [mH]	2.40 [mH]
Self-Induced Voltage : V_{rms}	4.92 [V]	3.81 [V]
Output : P	46.9 [W]	36.3 [W]
Torque : T	2.69 [Nm]	2.08 [Nm]
Power Factor : $\cos\theta$	0.99	0.90
Efficiency : η	0.83	0.76
Force Density : D	39.9 [kN/m^2]	30.9 [kN/m^2]
Frequency : f	50 [Hz]	50 [Hz]

As shown in Table I, the values of resistance and inductance in the experiment were larger than those in the theory. Therefore, actual specifications of the prototype motor were smaller than theoretical values. Table I shows each parameter at frequency 50 [Hz]. However, the prototype motor did not rotate smoothly and caused rattling noise at low frequency. In fact, the prototype motor could not rotate as a synchronous motor mode.

V. COGGING TORQUE REDUCTION

As the authors mentioned in previous section, the prototype motor could not rotate smoothly. The authors thought the reason that the prototype motor did not rotate well could be the cogging torque. The cogging torque is caused by the reluctance change between the stator teeth and magnet poles on the rotor. This is a characteristic of a PMSM often observed. The cogging torque causes excessive noise and harmful vibration to the machine itself, and in many serious cases, a mechanical resonance may occur which result in serious troubles. In many applications, the cogging torque has become an important design specification to be carefully treated. The cogging torque calculation and reduction method will be, therefore, discussed in this section.

A. Analytical Method to Calculate the Cogging Torque

There are many methods to calculate the cogging torque such as energy method, virtual work method, Maxwell tensor method etc [8]. Based on the energy method, the cogging torque can be calculated from the energy variation with the angle of rotation. In order to simplify calculation of the cogging torque, the authors have considered one pole-one core in the prototype model. The basic concept is considered without the flux leakage as illustrated in Fig. 17.

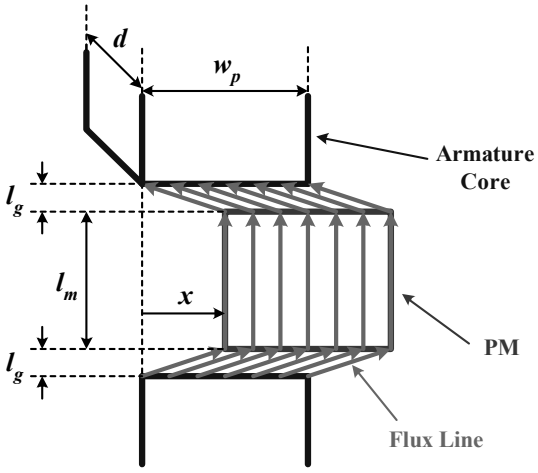

Fig. 17: The Simplified Flux Line in the Air Gap

In Fig. 17, l_g is the air gap length excepted magnet's height l_m, d and w_p are width and depth of both armature core and permanent magnet, and x is the length away from the initial position that magnet was below armature core vertically. Considering that magnet is in the initial position, the reluctance R_0 and flux density B_0 in the air gap are followed respectively,

$$R_0 = 2\frac{l_g}{\mu_0 S} + \frac{l_m}{\mu_0 S} \tag{11}$$

$$B_0 = \frac{H_c l_m}{R_0 S} = \frac{\mu_0 H_c l_m}{2l_g + l_m} \tag{12}$$

μ_0 is permeability of the air gap, H_c is the coercivity of magnet and S is the surface area of magnet. Considering that magnet is in x away from the initial position, the reluctance R_x and flux density B_{g_x} in the air gap are followed respectively,

$$R_x = 2\frac{\sqrt{x^2 + l_g^2}}{\mu_0 S} + \frac{l_m}{\mu_0 S} \tag{13}$$

$$B_{g\_x} = \frac{H_c l_m}{R_x S} = \frac{\mu_0 H_c l_m}{2\sqrt{x^2 + l_g^2} + l_m} \tag{14}$$

The total magnetic co-energy U_t in the air gap is followed as,

$$U_t = U_a + U_b = \frac{B_0^2}{2\mu_0} V_m + 2\frac{B_{g\_x}^2}{2\mu_0} V_g \tag{15}$$

U_a is the magnetic co-energy in the magnet when magnet is in the initial position. It is assumed that U_a is always constant. U_b is the magnetic co-energy in the gap at x away from the initial position. V_m, V_g are the volume of magnet and air gap. Therefore, the cogging torque F can be calculated as follows,

$$F = \frac{\partial U_t}{\partial x} = -4\mu_0 d w_p l_g H_c^2 l_m^2 \frac{x}{\sqrt{x^2 + l_g^2}\,(\sqrt{x^2 + l_g^2} + l_m)^3} \tag{16}$$

B. Method to Reduce the Cogging Torque

According to different applications and considerations of technical and economical factors, various cogging torque reduction methods can be employed, including Slot or magnet skewing (Fig. 18), Magnet pole shape optimization and Stator slot opening width optimization etc [8]. In particular, skewing has been well recognized as a practical technique to reduce the cogging torque of PMSM. In this paper, the authors calculated the cogging torque as a

function of skewing angle of the magnets. Considering the skewing, the cogging torque is expressed as (17).

$$F = -\frac{4\mu_0 w_p l_g (H_c l_m \cos\theta)^2}{\theta} \cdot \frac{2xd\theta + l_m\{A-B\}}{\{2B+l_m\}^2\{2A+l_m\}^2} \qquad (17)$$

$$A = \sqrt{\left(x+\frac{1}{2}d\theta\right)^2 + l_g^2}\ ,\quad B = \sqrt{\left(x-\frac{1}{2}d\theta\right)^2 + l_g^2}$$

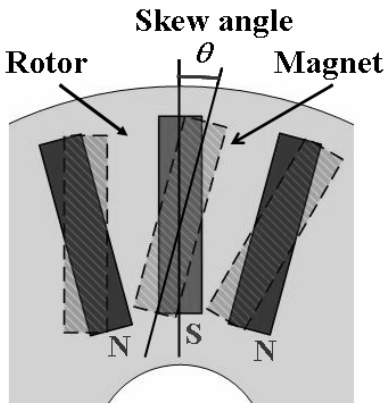

Fig. 18: Skew Angle

Considering the geometric structure, the authors decided the skew angle θ as 4 [deg]. According to variation of skew angle, the cogging torque is shown in Fig. 19. When not considering skewing, the cogging torque was 51 [N] and its peak value was at 0.6 [mm] from the initial position. In 4 [degree], although it was not eliminated perfectly, the cogging torque was 28 [N] and its peak value was at 1.8 [mm] from the initial position. The cogging torque decreased to almost half by skewing.

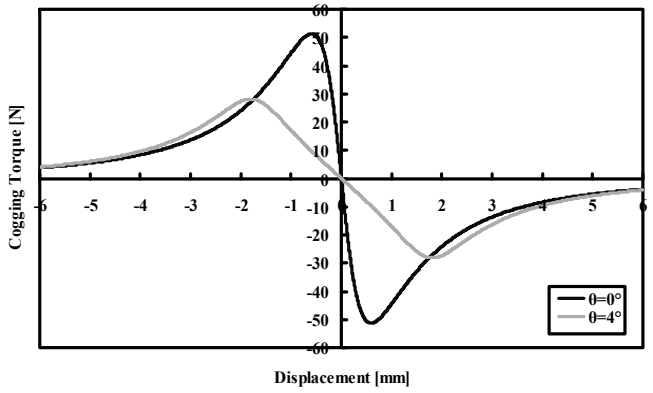

Fig. 19: Cogging Torque per a Pole Depending on Skew Angle

VI. CONCLUSIONS

This paper proposed a new evolution in the development of the transverse flux type permanent magnet motor. A new idea for a low-speed, high-torque permanent magnet motor was proposed. The authors reviewed the initial transverse flux concept and two adaptations of the TFM topology. In Section II, a new design of the proposed motor was described as a modification of the TFMs. It has a simple flux topology that allows for simplified linear modeling of the motor characteristics.

The fundamental measurements of the prototype's open circuit voltage armature impedance and self-induced voltage were completed in experiment. Also, the fundamental characteristics of the prototype motor were estimated analytically and compared with experiment values. However, some empirical values are estimated based on R, L, V_{rms} by equations that the authors have used to calculate theoretical data because the prototype motor could not be rotated as synchronous motor mode.

The authors thought the reason that prototype motor did not rotate well could be the cogging torque. In Section III, in order to solve the problem, the cogging torque was calculated as a function of skewing angle of the magnets. By an appropriate skewing, the cogging torque can be reduced to half theoretically.

The new model, *i.e.*, the second model, is being fabricated. In particular, the number of armature core, winding, and pole were changed in order to gain a higher torque than first model. Skewing was also considered in order to decrease the cogging torque.

VII. ACKNOWLEDGMENT

We would like to thank MT-Drive (MTD) and Japan Society for the Promotion of Science (JSPS) for their friendly support to this research.

VIII. REFERENCES

[1] Borman, J., Sharman, B., "Electric Propulsion of Passenger Ships and Other Vessels," *Trans. ImarE,* pp. 77-104, 16 Nov. 1993.

[2] ABB, "ABB Marine – References," *www.abb.com/marine*, Center of Excellence Cruise & Ferries: ABB Oy, Helsinki, Finland, December 2006.

[3] Harris, M.R., Pajooman, G.H., Abu Sharkh, S.M., "The Problem of Power Factor in VRPM(Transverse-Flux) Machines," *IEEE Conference on Electrical Machines and Drives 1997,* Publication No. 444, IEEE, Sept. 1997.

[4] Weh, H, Hoffman, H, Landrath, J, "New Permanent Magnet Excited Synchronous Machine with High Efficiency at Low Speeds," *Proceedings of the International Conference on Electrical Machines,* 1988.

[5] Kim, HJ, Nakatsugawa, J, Sakai, K, Shibata, H, "High-Acceleration Linear Motor, "Tunnel Actuator"," *The Magnetics Society of Japan,* Vol. 29, No. 3, pp 199-204, 2005.

[6] Husband, S.M., Hodge, C.G., "The Rolls-Royce Transverse Flux Motor Development," *Electric Machines and Drives Conference*, Vol. 3, pp. 1435-1440, IEEE, 2003.

[7] G. Patterson, T. Koseki, Y. Aoyama, K. Sako,"Simple Modeling and Prototype Experiments for a New High-Thrust, Low-Speed Permanent Magnet Disk Motor," Proc. *12th International Conference on Electrical Machines and Systems*, Tokyo, Japan. Nov 2009.

[8] Z. Guo, L. Chang, Y. Xue, "Cogging torque of permanent magnet electric machines: an overview," *Canadian Conference Electrical and Computer Engineering*, CCECE '09, pp. 1172-1177, 2009.